Theoretical analysis of Raman spectra of finite-stage Si/Si-Ge Fibonacci superlattices

G. C. Aers and M. W. C. Dharma-wardana
Division of Physics, National Research Council, Ottawa, Canada K1A 0R6

G. P. Schwartz and J. Bevk
AT&T Bell Laboratories, Murray Hill, New Jersey 07974-2070
(Received 31 August 1988)

Raman-scattering results for acoustic phonons in Si/Ge_xSi_{1-x} Fibonacci superlattices with low-stage numbers are analyzed and shown to have significant deviations from the infinite-stage assumption implicit in standard theoretical models. We show that a quantitative description of the observed spectra is possible only with a "sample-specific" theory which takes into account the presence of the substrate and the free surface. A nearest-neighbor linear-chain model is used to calculate Raman spectra which are in good agreement with experiment.

I. INTRODUCTION

With the advent of growth techniques such as molecular-beam epitaxy, it has been possible to study the lattice-dynamical properties of zone-folded acoustic phonons in both periodic and quasiperiodic structures. Quasiperiodic lattices are rather unique in several ways. For example, such structures will exhibit a dense distribution of peaks throughout the allowed acoustic frequency spectrum rather than the evenly spaced doublets found in periodic superlattices. In addition, the allowed acoustic frequencies will depend on the size or stage number of the lattice. It is thus possible to observe size-dependent frequency shifts in finite quasiperiodic structures whereas periodic superlattices are expected to primarily exhibit peak broadening in equivalent-sized structures.

The theory of light scattering from periodic[1] and quasiperiodic superlattices[2,3] proceeds by imposing periodic boundary conditions appropriate to an infinitely "large" superlattice. Experimental Raman spectra of large superlattices reveal zone-folded phonon excitations and are generally in good agreement with the theory based on periodic boundary conditions (PBC) for a superlattice with infinitely many repeats. However, in "low-stage" superlattices, i.e., superlattices where the number of "repeats" is too small to be treated as being "infinite," the experimental spectra[4,5] begin to show marked deviations from PBC and a more "sample-specific" theory becomes necessary. In fact, in discussing the Raman spectrum of acoustic phonons in ultrathin multilayer structures (MLS) of the type $(Ge)_m/(Si)_n$, where $m,n<6$, it has been shown that the observed Raman spectrum can be interpreted only if the surface boundary conditions and the presence of the substrate are explicitly included in the calculation. Both the experimental results and the calculation showed that the continuum of phonons associated with the substrate interact with the long-wavelength modes of the MLS to produce strong changes in the intensity of the Brillouin peak and generated new, broad, intense peaks which were interpreted as "resonant" phonon modes.[5,6]

In this report we present a theoretical analysis of Raman-scattering results[4] for $Ge_{0.2}Si_{0.8}/Si$ multilayer structures of low-stage Fibonacci superlattices grown by molecular-beam epitaxy on Si(001) substrates. The Fibonacci structures are made by juxtaposing two materials, A and B, so that the nth-stage superlattice S_n is given iteratively by the concatenation rule $S_n=S_{n-1}S_{n-2}$, for $n\geq 3$, with $S_1=A$ and $S_2=AB$, $S_3=ABA$, $S_4=ABAAB$, etc. In Sec. II we will present the low-frequency Raman spectra for sixth-, eighth-, and tenth-stage Fibonacci structures, having, respectively, 13, 34, and 89 type-A and -B blocks. The tenth-stage Fibonacci structure with 89 blocks contains 55 blocks of type A and 34 blocks of type B and hence contains a total of 2445 monolayers deposited on the Si substrate. Even in this case, although the positions and intensities of most of the peaks are well predicted by the analytic theory based on the infinite-stage result, the low-frequency end close to the Brillouin peak shows disagreement which can be corrected only when a sample-specific calculation involving the substrate and the surface boundary conditions is carried out. To make a detailed sample-specific theory we model the substrate and MLS with specific boundary conditions using a linear-chain model developed in Sec. III. Such linear-chain models are valid for the [001]-growth-direction dynamics and the light-scattering experiments reported here are designed to probe vibrational properties along this direction. Results from these calculations are presented and concluding remarks are made in Sec. IV.

II. RAMAN SPECTRA FOR THE LOW-STAGE FIBONACCI LATTICES

In order to study the progression towards full quasiperiodicity and to unravel finite-sample effects we have modeled experimental Raman spectra of Fibonacci superlattices of stage N (i.e., S_N), with $N=6$, 8, and 10. These structures have the triplet structure

$S_6 = S_4 S_3 S_4$,

$S_8 = S_6 S_5 S_6$,

$S_{10} = S_8 S_7 S_8$,

with $S_3 = ABA$, $S_4 = ABAAB$, and $S_N = S_{N-1} S_{N-2}$. The type-A blocks, being of $Ge_{0.2}Si_{0.8}$ have a small lattice mismatch of about 0.84% with respect to the Si substrate and the type-B layers which are also of pure Si. Note that all the samples studied here (i.e., S_6, S_8, and S_{10}) have an end surface (top surface) of material B (i.e., Si).

The Raman spectra were obtained with 5145- Å excitation at room temperature with the samples under vacuum in a backscattering geometry. Data collection times varied from 20 to approximately 80 h depending on the stage number of the sample. The power at the sample was 300 mW. The raw spectra have been reported previously in Ref. 4.

In Fig. 1 [panel a] we present the low-frequency part ($\omega < 50$ cm^{-1}) of the fitted experimental Raman spectrum for the Fibonacci superlattice S_{10}. The raw data were fitted to a series of Gaussian peaks with use of a nonlinear least-squares routine in which the amplitudes, frequencies, and half-widths were parameters. The Rayleigh-Brillouin wing and dark noise background were approximated using a fit with five additional parameters in the functional form $c_1 + c_2 e^{-c_3\omega} + c_4 e^{-c_5\omega}$. Various functional forms for the background were examined, but the form employed above proved to be the most consistent when applied to all the data sets. Nevertheless, the process of removing the Rayleigh-Brillouin wing is not unique, and both the width and intensity of the shoulder on the wing seen around 10 cm^{-1} varies between fits with equal constrained error specifications by slightly varying the background parameters. This should be borne in mind when viewing the essential parts of the spectra with background removed as shown in the a panels of Figs. 2–4. Although the intensity of the first peak at $\omega \approx 10$ cm^{-1} is sensitive to the functional form used to remove the background and the Rayleigh-Brillouin scattering, we believe that the relative intensities in the S_6, S_8, and S_{10} cases are reasonably well accounted for. If we ignore the $\omega \approx 10$ cm^{-1} peak for the moment, we note that the S_6 spectrum is radically different from the S_{10} spectrum, both in its qualitative appearance and in its detailed structure. The S_8 spectrum is qualitatively closer to the S_{10} spectrum.

Panel d of Figs. 2–4 shows the spectrum calculated in the usual manner, by assuming that we can replace the finite S_N-Fibonacci problem by an infinite periodic superlattice where the repeating subunit is the finite multilayer structure given by S_N. We shall denote this *PBC* model by $S_N^{(P)}$. The spectrum for $S_N^{(P)}$ can be calculated, assuming a step-function variation of the photoelastic constants P_A and P_B for the phonons as in Ref. 2. The calculation can be done numerically by evaluating Eq. (2) of Ref. 2. Alternatively, an analytic formula similar to Eq. (10), Ref. 2 can be derived[7] via the projection technique by

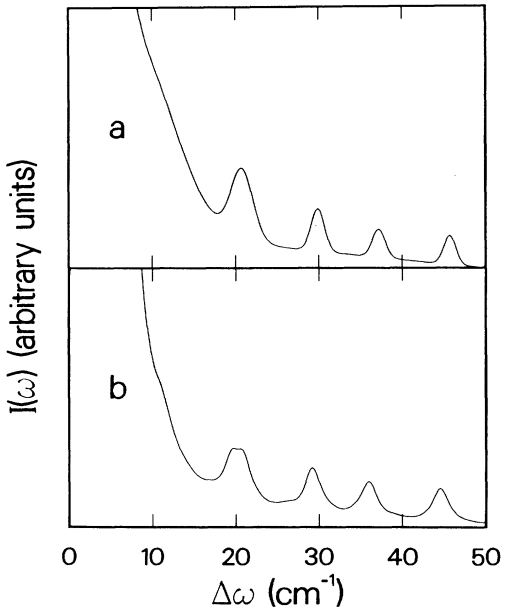

FIG. 1. Smoothed Raman spectrum obtained from nonlinear least-squares curve fitting (panel a) for the tenth-stage Fibonacci structure taken with 5145-Å excitation. The instrument resolution was 2.5 cm^{-1}, and the Rayleigh-Brillouin wing has not been removed. Panel b shows a calculated Raman spectrum for a finite Fibonacci lattice using the linear-chain model including 1000 monolayers of substrate and a free-surface ($\sigma = 0$) boundary condition.

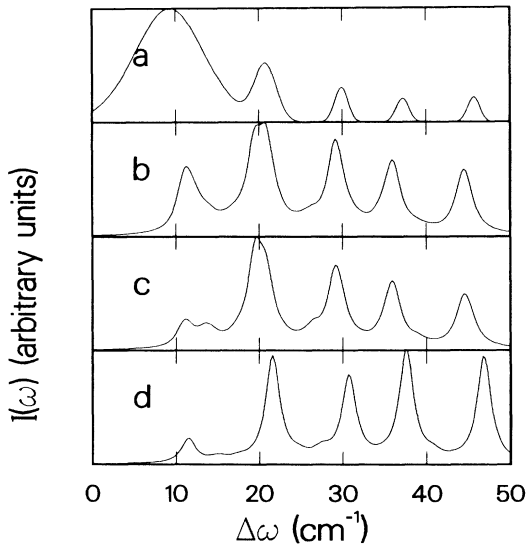

FIG. 2. Curve fitted and calculated Raman spectra for the tenth-stage Fibonacci structure. Panel a shows the smoothed spectrum without the Rayleigh-Brillouin wing. Panels b and c show calculations using the linear-chain model which includes substrate and surface boundary effects: b, free surface, $\sigma = 0$ in Eq. (2) of text; c, anchored surface, $\sigma = 1$. Panel d shows the periodic approximation $S_{10}^{(P)}$.

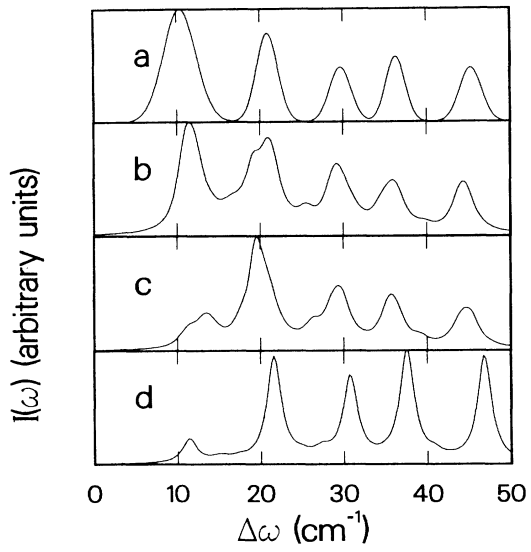

FIG. 3. Curve fitted and calculated Raman spectra for the eighth-stage Fibonacci structure. Panel *a* shows the smoothed spectrum without the Rayleigh-Brillouin wing. Panels *b* and *c* show calculations using the linear-chain model which include substrate and surface boundary effects: *b*, free surface; *c*, anchored surface. Panel *d* shows the periodic approximation $S_8^{(P)}$.

choosing the projection axis ξ (axis and notation of Fig. 2, Ref. 2) such that $\cot^2\theta = F_{N-1}d_A/(F_{N-2}d_B)$ where d_A and d_B are the lengths of the type-A and- B blocks while F_{N-1} and F_{N-2} are the Fibonacci numbers corresponding to the number of type-A and -B blocks, respectively, in the Nth stage Fibonacci lattice (for example, for $N=8$, $F_{N-1}=21$, and $F_{N-2}=13$). In other words, the projection using the irrational number $\tau=(1+\sqrt{5})/2$ is replaced by the rational approximation F_{N-1}/F_{N-2} [$(N-1)$th convergent] corresponding to the stage N. The width of the projection strip also has to be adjusted in the same manner. Panel *d* of Figs. 2–4 was obtained by direct numerical evaluation, including a Lorentzian broadening of 1 cm^{-1}, and it is clear that the calculated spectra are essentially independent of the stage number N (for sufficiently large N). That is, $S_6^{(P)}$ is already very similar to $S_N^{(P)}$ where $N\to\infty$. Thus the theory of the periodically extended S_N-Fibonacci subunit is of little value in explaining the observed experimental progression shown in panel *a* of the figures. Even the spectrum of S_{10} with 2445 monolayers is poorly predicted by the standard theory [i.e., the $S_{10}^{(P)}$ model] in that the intensities are manifestly incorrect. Straightforward elaborations of the model involving, say, replacement of the continuum approximation for the phonon modes by an explicitly calculated mode spectrum for the $S_{10}^{(P)}$ helps marginally, but the experimental spectra demand a more sample-specific theory.

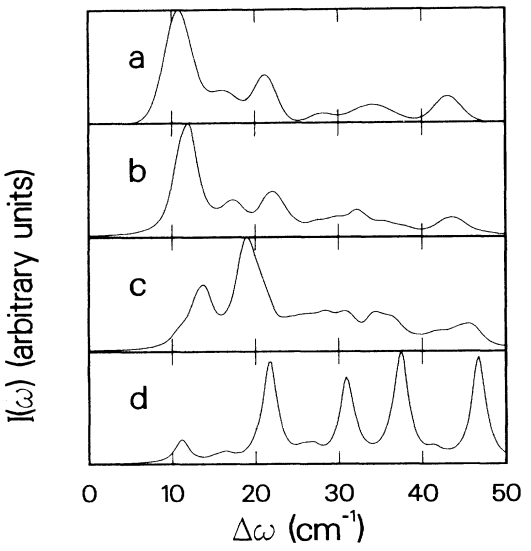

FIG. 4. Curve fitted and calculated Raman spectra for the sixth-stage Fibonacci structure. Panel *a* shows the smoothed spectrum without the Rayleigh-Brillouin wing. Panels *b* and *c* show calculations using the linear-chain model which include substrate and surface boundary effects: *b*, free surface; *c*, anchored surface. Panel *d* shows the periodic approximation $S_6^{(P)}$.

III. THE LINEAR-CHAIN MODEL

The Raman spectra of ultrathin multilayer structures grown on Si[001] substrates were discussed in Ref. 5. The interpretation of the experimental spectra required a sample-specific theory where the presence of the substrate as well as a capping layer sandwiching the multilayer structure (MLS) was explicitly taken into account. In the present problem we have a substrate and MLS, but no capping layer. However, the top layer of the MLS establishes a surface boundary condition on the vibrational problem. Similarly the Fourier transformations involved in the light-scattering problem now involve a *finite domain* extending from the surface layer (top of the MLS) to the first monolayer of the substrate.

To model the longitudinal-phonon spectrum along the [001] direction we use a linear-chain model[6] with nearest-neighbor coupling f. Thus in the present problem we have f_B for interactions between two neighboring Si monolayers of mass m_B and similarly f_A for the alloy layers of average mass m_A. The first Si atom (i.e., monolayer) of the substrate is assumed to be fully anchored, with an equation of motion

$$m_B\ddot{z}_1 = f_B(z_2-z_1)-f_Bz_1 , \tag{1}$$

where z is the growth direction, and m_B is the mass of the first substrate monolayer (Si atom). Note that z_1, z_2, etc., are the longitudinal *displacements* of the respective atomic layers. The equation of motion of the surface monolayer v is given by

$$m_v\ddot{z}_v = f_B(z_{v-1}-z_v)-f_Bz_v\sigma , \tag{2}$$

where we have introduced a parameter σ which could be set to zero for a completely free surface, while an anchored surface would require σ to be unity (since the actual surface may be oxidized or otherwise affected, the value of σ may be some value different from zero even for

a nominally free surface).

Since we are interested in the long-wavelength phonon spectrum ($\omega < 50$ cm^{-1}) further simplification in Eqs. (1) and (2) can be made. For instance, instead of writing f_A and f_B in the type-A and -B layers of the multilayer part, and average values $f_{AB}=0.5(f_A+f_B)$ for the bonds across an A-B interface, we used an average force constant f for the coupling between any two monolayers in the whole structure. The substrate was modeled by l_S layers of Si with $l_S=1000$. The value of f was fixed by choosing it to reproduce the experimental Brillouin frequency ($\omega \approx 5.3$ cm^{-1}) and was found to be 1.616×10^5 dyn/cm, as compared with the "bulk" value of 1.8×10^5 dyn/cm. If l_S were increased, f increases slowly towards the bulk value. We have retained $l_S=1000$ in the following calculations to keep the dynamical problem small. The substrate plus MLS will contain $L=l_S+l_{\rm MLS}$ layers. Thus, for the tenth-stage Fibonacci structure we have $L=3445$ with $l_S=1000$ for the substrate. The $L\times L$ matrix defining the dynamical problem is tridiagonal and can be easily solved to give the mode frequencies ω_j and the mode amplitudes $u_j(z)$.

The nominal thicknesses based on x-ray diffraction were 44.0 Å (32 monolayers) for A and 29.9 Å (22 monolayers) for B. The best fit to experiment, from the present study, gives 29 and 25 monolayers, respectively, for type-A and -B layers. It should be noted, however, that the discrepancy between the x-ray diffraction block width determination and the values used in the fits are model dependent insofar as only one force constant is used in the linear-chain model to describe both the Ge_xSi_{1-x} and Si layers. In effect the layer widths serve as *de facto* fitting parameters.

The theoretical Raman spectrum is calculated with use of the modes ω_j, amplitudes $u_j(z)$, and a photoelastic coupling mechanism. That is, if the change in the photon momentum in the Raman scattering is q, the intensity of the Raman scattered light is given by

$$I(\omega)\propto\sum_j\frac{\Gamma/\pi}{(\omega-\omega_j)^2+\Gamma^2}\left[\frac{n(\omega_j)+1}{\omega_j}\right]\times\left|\int_0^d e^{-iqz}P(z)\frac{\partial u_j(z)}{\partial z}dz\right|^2, \quad (3)$$

where Γ is a broadening parameter (≈ 1 cm^{-1}) and $n(\omega_j)$ is the Bose factor. The Fourier transform extends from $-\infty$ to $+\infty$ in the usual theory, but here, the total length of the structure consisting of $l_S+l_{\rm MLS}$ layers is $d=a_{\rm Si}l_S+d_{\rm MLS}$ where $a_{\rm Si}$ is the silicon monolayer thickness (1.36 Å), while $d_{\rm MLS}$ is the thickness of the multilayer structure. Since the multilayer structures were made up of $Ge_{0.2}Si_{0.8}$ blocks and pure Si blocks, the monolayer thickness everywhere is essentially almost the same as in pure Si. The calculated spectrum is found to be insensitive to local variations in the monolayer thickness just as it was found adequate to use an average force constant f instead of f_A, f_B, and f_{AB} over the range of frequencies considered here. In Eq. (3) the photoelastic coupling constant is $P(z)$, and takes an arbitrary constant value of P_B in the silicon substrate, and in the silicon layers (type-B blocks), while a value of P_A is assigned to the $Ge_{0.2}Si_{0.8}$ layers (type-A blocks). Values of 1000 and 500 were used for P_A and P_B, respectively. The intensity is mostly controlled by the ratio P_B/P_A, while the force constants and the surface boundary condition (parameter σ) also play a role via their effect on the phonon spectrum.

IV. DISCUSSION OF RESULTS

In this section we compare the prediction of the linear-chain model with the curve-fitted experimental spectra. The calculated spectra for the Fibonacci structures with ten, eight, and six stages are shown in panel b of Figs. 2–4, respectively, with the surface layer taken to be completely free ($\sigma=0$). In panel c we show the results of the calculation if the surface monolayer is assumed to be anchored ($\sigma=1$). It is clear that the spectrum calculated using the free-surface boundary condition gives good agreement with the experimental spectrum in all three cases, where the same force constant and layer thicknesses (for layers A and B) are used in all three calculations. The large width of the first peak (≈ 10 cm^{-1}) in Fig. 2 (experimental curve) is partly an artifact of the procedure used to remove the background Rayleigh and Brillouin wings. If we return to Fig. 1, panel b shows the calculated S_{10} spectrum inclusive of the Rayleigh-Brillouin wing, to be compared with the full experimental spectrum of panel a of the same figure. The calculated spectrum is for the free surface boundary condition

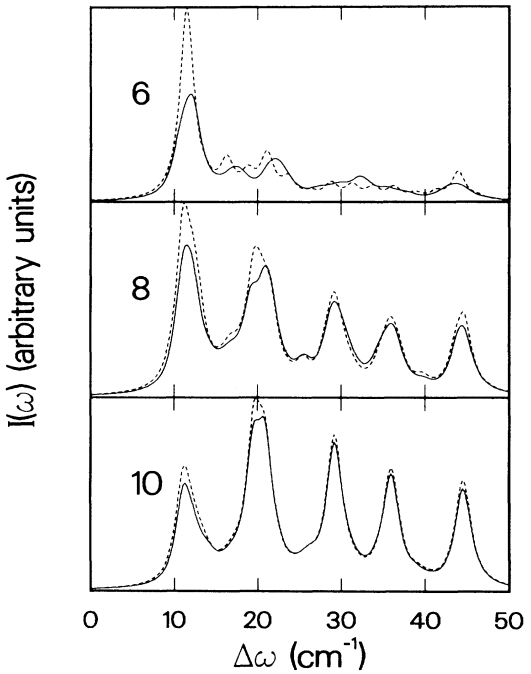

FIG. 5. Comparison of spectra calculated with use of the linear-chain model with substrate (solid curves) and without substrate (dashed curves) for sixth-, eighth-, and tenth-stage Fibonacci superlattices including a free-surface boundary condition ($\sigma=0$).

($\sigma=0$).

In Ref. 5, where $(Ge)_m/(Si)_n$ ultrathin superlattices were studied it was found that the outer surface (Si) of the MLS had to be modeled as a slightly constrained ($\sigma=0.1$) surface rather than a free ($\sigma=0$) surface. In the present MLS the outer surface is also a Si layer. Unlike Ref. 5, here we find the best agreement with experiment using the free-surface boundary condition $\sigma=0$.

In order to understand the role of the substrate we have calculate the Raman spectrum with and without the substrate, with the first (bottom) layer anchored and the surface (top) layer free ($\sigma=0$). The results of the calculations are shown as solid (with substrate) and dashed (without substrate) curves in Fig. 5 for S_6, S_8, and S_{10}. The calculation for S_{10} shows that a finite multilayer without a substrate, but with the free-surface boundary condition, is better than the $S_{10}^{(P)}$ calculation shown in panel *d* of Fig. 2. In the case of S_6 we see that an extremely high intensity attributed to the $\omega\approx 10\text{-cm}^{-1}$ peak is moderated by the presence of the substrate and enhanced by the presence of the free surface.

In conclusion, we have shown that even for relatively large-stage multilayer structures like a tenth-stage Fibonacci superlattice, the Raman spectrum at the low-frequency end is sensitive to sample-specific aspects associated with the surface boundary conditions and the presence (or absence) of the substrate. The sample specificity appears both in the calculation of the phonon modes and amplitudes, and also in the calculation of the intensity via the photoelastic coupling model.

[1]L. Colvard, R. Merlin, M. V. Klein, and A. C. Gossard, Phys. Rev. Lett. **45**, 298 (1980); Jianjun He, B. Djafari-Rouhani, and J. Sapriel, Phys. Rev. B **37**, 4086 (1988).

[2]M. W. C. Dharma-wardana, A. H. MacDonald, D. J. Lockwood, J.-M. Baribeau, and D. C. Houghton, Phys. Rev. Lett. **58**, 1761 (1987).

[3]R. Merlin, K. Bajema, R. Clarke, F. Y. Juang, and P. K. Bhattacharya, Phys. Rev. Lett. **55**, 1768 (1985).

[4]A. T. Macrander, G. P. Schwartz, and J. Bevk, Phys. Rev. B **37**, 8459 (1988).

[5]D. J. Lockwood, M. W. C. Dharma-wardana, G. C. Aers, and J.-M. Baribeau, Appl. Phys. Lett. **52**, 2040 (1988).

[6]A. S. Barker, Jr. and A. J. Sievers, Rev. Mod. Phys. **47**, S1 (1975); see also A. Fasolino and E. Molinari, J. Phys. (Paris), Colloq. **48**, C5-569 (1987).

[7]R. K. P. Zia and W. J. Dallas, J. Phys. A **18**, L341 (1985). Note that the projection method given here has to be modified as in Ref. 2 if a Fibonacci sequence starting from the origin as $ABAAB\ldots$, etc., is to be obtained.